# Converging narrow-channel flow of a super-critical fluid

Abdallah El Malki [a], Roger E. Khayat [b], Sakir Amiroudine [a,*]

[a] Univ. Bordeaux, CNRS, Bordeaux INP, Arts et Métiers Paris Tech, I2M UMR 5295, Talence, F-33400, France
[b] Department Mechanical and Materials Engineering, Western University, Canada

*Keywords:*
Supercritical fluid
Compressible
Lubrication
van der Waals
Poiseuille

The solution of a supercritical fluid flowing into a constricted narrow channel is presented in this study. The compressible Navier-Stokes equations in the lubrication limit coupled with the energy equation and the isothermal and non-isothermal van der Waals fluid and perfect gas have been solved. In order to find the semi-analytical solution of these non-linear coupled equations, homogenization technique in the transverse direction has been applied. Because of the high compressibility and high thermal expansion of supercritical fluids, waviness is observed in the flow and thermal fields near the exit of the channel. This effect is attributed to the channel constriction where the slope is maximum, where a strong coupling between the pressure and density gradients exists. Moreover, the density difference between the exit and inlet of the channel drastically increases when one approaches the critical point, corroborating the data from existing literature.

## 1. Introduction

Supercritical fluids (SCFs) are a class of fluids that exist beyond the liquid-vapor critical point and may be considered as an intermediate state between a liquid and a gas. They exhibiting some properties of liquids, like high density and solubility, and some properties of gases such as low viscosity and high compressibility [1]. On approaching the critical point, the various thermo-physical properties show a singular behavior such as diverging isothermal compressibility, heat conductivity, specific heat at constant pressure and constant volume, and a vanishing thermal diffusivity [2,3]. These properties have been found to behave according to the universal power laws with a different critical exponent for each property. They can be modelled on the basis of a common parameter $\delta = \frac{T_i - T_c}{T_c}$, where $T_c$ refers to the critical temperature and $T_i$ is the initial temperature of the fluid. The most unusual behavior (and new at that time) of near-critical fluids was observed by Nitsche & Straub [4] during the measurement of the heat capacity at constant volume in their sounding rocket experiment. They observed that the thermalization of their cell was extremely fast despite a vanishing thermal diffusivity. Three worldwide independent teams have [5–7] explored this unusual phenomenon and explained that this phenomenon of critical acceleration of heating due to the *piston effect*, attributed to the high compressibility and thermal expansion near the critical point. A new timescale, called the piston-effect timescale has been defined which vanishes at the critical point and the tiny remaining thermal non-homogeneity is achieved by the very slow heat diffusion (the thermal diffusivity vanishes near the critical point).

These unique properties make supercritical fluids ideal candidates for various industrial processes and lubrication systems [8,9]. The modeling of microscale critical region flows and heat transfer mechanisms continues to be a challenging task in both theoretical research and engineering applications. Recently, the study of a flow in a micron-sized capillary has been considered in Refs. [10,11]. This flow is characterized by a trans-critical pressure in the microcapillary and is at the critical temperature at the channel walls.

Supercritical fluids have many applications in aerospace lubrication systems involving thin constrictions mainly in turbomachinery [12,13]. In aerospace engineering, lubrication is essential for reducing friction and wear between moving components, ensuring smooth operation, and extending the lifespan of critical parts. In aerospace machinery and mechanisms, thin film lubrication is often employed to create a protective layer between sliding surfaces. Supercritical fluids offer advantages in thin film lubrication due to their unique properties, such as high density and low viscosity near the critical point. These properties allow supercritical fluids to form thin and robust lubricating films, even in constricted regions and under varying working conditions [2]. Thin constrictions in lubrication systems, such as bearing gaps and sliding interfaces, pose challenges for traditional lubricants. However, supercritical fluids can adapt to such complex geometries, ensuring efficient lubrication and minimizing wear and frictional losses in aerospace components. The utilization of supercritical fluids as lubricants in thin

* Corresponding author.
*E-mail address:* sakir.amiroudine@u-bordeaux.fr (S. Amiroudine).

https://doi.org/10.1016/j.ijthermalsci.2024.109553

**Nomenclature**

*Dimensionless variables and parameters*

| | |
|---|---|
| $A$ | cohesion factor |
| B | molar covolume |
| $c_p$ | non-dimensional heat capacity at constant pressure |
| C | ratio of the reference pressure to the reference shear stress |
| Ec | Eckert number |
| h(x) | variable channel height |
| k | thermal conductivity |
| p | pressure |
| *Pe* | Peclet number |
| Pr | Prandtl number |
| Re | Reynolds number |
| T | temperature |
| <T> | average temperature in the streamwise direction |
| u | velocity component in the x-direction |
| v | velocity component in the y direction |
| x | longitudinal direction |
| y | transverse direction |

*Greek symbols*

| | |
|---|---|
| β | thermal expansion coefficient for a supercritical fluid |
| ρ | density |
| ε | channel height-to-length ratio |
| δ | proximity to the critical point |
| $\boldsymbol{\gamma}$ | rate-of-strain tensor |
| $\boldsymbol{\tau}$ | viscous stress tensor |

*Subscripts*

| | |
|---|---|
| c | critical value |
| r | reference value |
| 0 | perfect gas value |

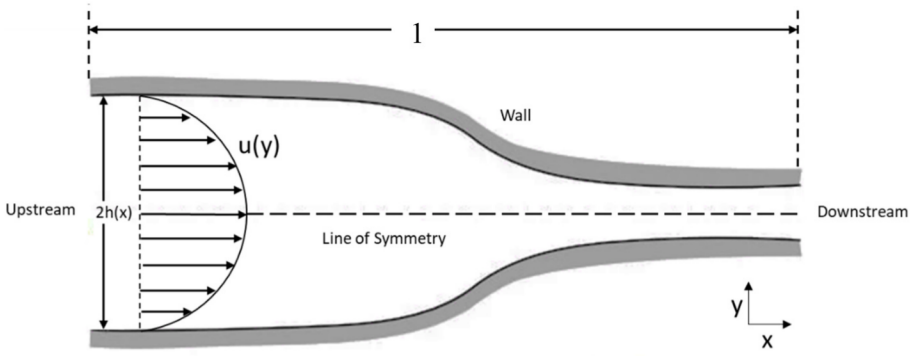


**Fig. 1.** Geometry of the channel. At the inlet the pressure is imposed yielding a parabolic velocity profile. The height H is taken as the half-height at the inlet, and L is the channel length, the channel variable height is 2 h(x) (in units of H).

constrictions holds the potential to enhance the reliability, efficiency, and performance of aerospace machinery and mechanisms. However, understanding the behavior of these fluids is complex.

In all these applications, the flow can be operated in different forms of tubes (regular and singular) and in the configuration of Poiseuille or Couette flows. These variable geometry channels, such as nozzles, ducts, and heat exchangers, offer opportunities to manipulate flow patterns, enhance heat transfer, and minimize pressure drop. However, the presence of complex flow patterns and thin gaps poses challenges in accurately modeling the fluid behavior in such scenarios.

This study focuses on the flow of a supercritical fluid in a narrow contracting channel. Narrow channel contracting flow constitutes an ideal configuration from fundamental and practical perspectives. Lubrication theory is typically adopted to incorporate the large normal stress that results from contraction. In such narrow channels, the walls can influence the flow characteristics and form secondary currents. These vortex structures can alter the longitudinal velocity distribution and form velocity dip. For this reason, narrow channel flows have been examined under various conditions, including complex fluid flow [14, 15]. Of closer relevance to supercritical fluids, one of the most effective techniques to combat reservoir sedimentation is the installation of Sediment Bypass Tunnels, which are designed for supercritical narrow open channel flow conditions. They can also alter the bed shear stress distribution and influence the sediment transport [16].

Our model is based on the Reynolds compressible Stokes equations, coupled with the equation of state and energy equation, allowing for a simple modelling and comprehensive understanding of the fluid flow behavior, including pressure, heat dissipation and flow field variations along the length of the channel. To comprehensively assess the predictive capability of the analytical model, a comparative analysis is performed between perfect gas (PG) and van der Waals (vdW) fluids both in isothermal and non-isothermal situations. The comparison aims to elucidate the differences in the behavior of supercritical fluid and perfect gas under various modeling assumptions and to identify the strengths and limitations of each modeling approach for fluid dynamics applications. Several limitations and assumptions are carefully considered to ensure the validity and applicability of the model. One significant limitation lies in the thin film theory employed to model lubrication in the variable geometry channels. While the thin film approximation is well suited for analyzing fluid flow in thin gaps and constrictions, it assumes a continuous and uniform lubricating film, neglecting potential fluctuations and instabilities that may arise in real-world scenarios, and puts a constraint on the type of geometry where this model can be applied to. Another essential assumption lies in the simplifications made to the Navier-Stokes and energy equations. To facilitate the solution, certain terms such as the inertial terms are omitted with some well-posed assumptions. Furthermore, the model incorporates the Reynolds compressible equation, which follows a simplified equation of state (vdW) and the solution is obtained by averaging the temperature field in the transverse direction. These assumptions are reasonable for flows in the proximity of the critical point, they capture the complexities of non-isothermal flows. Section 2 presents the problem formulation and the mathematical approach for solving the governing equations and boundary conditions. Sections 3 and 4 present the results of PG and vdW

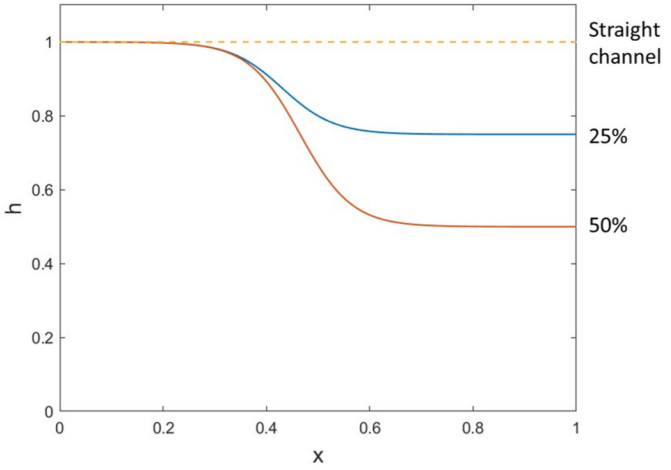


**Fig. 2.** Graphical representation of the channel height, h(x), following equation (2.11) for three different reductions (straight channel, 25 % and 50 % reductions).

fluids, respectively, for both isothermal and non-isothermal cases. Concluding remarks are given in section 5.

## 2. Problem formulation

### 2.1. Geometry of the contracting flow

In this work, we follow Rothstein & McKinley [9] and explore the pressure drop originating from the non-uniformity of geometry while eliminating the entrance and exit effects. We examine the contracting flow in a 2D channel consisting of a slowly spatially varying and symmetric domain. In this case, H is taken as the half-height at the inlet, and L is the channel length between the inlet and outlet locations. The channel variable height is 2h(x) (in units of H). The physical domain is therefore connected to two long straight channels of half-height h (x = 0) = 1 at the inlet, and height h (x = 1) = α < 1 at the outlet (see Fig. 1).

The channel height is taken as a function of x, h(x), following the equation:

$$h(x) = -\frac{1}{a + e^{-b(x-c)}} + 1 \tag{2.1}$$

where "a" represents the percentage decrease in the inlet height (i.e. for example a = 4 represents a 25 % decrease in the inlet height, a = 2 represents a 50 % decrease), "b" represents the gradient or the steepness of the height drop, "c" represents the midpoint of the function or the channel (for example c = 0.5 indicates that the midpoint of the function is at the midpoint of the channel).

Fig. 2 shows three examples of the symmetric channel profile, h(x), used in this study where the flow equations are solved for a straight channel, a converging channel with 25 % reduction and 50 % reduction with respect to the initial height corresponding to the value of a = 4 and a = 2, respectively.

### 2.2. General compressible flow equations

In the absence of gravity effect, the general steady compressible conservation equations along with the gas equation of state are [17]:

$$\nabla \cdot (\rho \mathbf{v}) = 0, \tag{2.2a}$$

$$\rho \mathbf{v} \cdot \nabla \mathbf{v} = -\nabla p + \nabla \cdot \boldsymbol{\tau}, \tag{2.2b}$$

$$\rho c_p \mathbf{v} \cdot \nabla T = \nabla \cdot (k \nabla T) + \beta T \frac{dp}{dt} + \boldsymbol{\tau} : \boldsymbol{\gamma}, \tag{2.2c}$$

$$p = p(\rho, T), \tag{2.2d}$$

where ρ is the fluid density, **v** is velocity vector, T is temperature, p is the gas pressure, $\boldsymbol{\tau}$ is the viscous stress tensor, **I** the identity tensor, $\boldsymbol{\gamma}$ is the rate-of-strain tensor, $c_p$ is the specific heat at constant pressure, k is the coefficient of thermal conductivity, t is the time. $\frac{d}{dt} = \mathbf{v} \cdot \nabla$ is the material derivative. Here $\beta = -\frac{1}{\rho}\left(\frac{\partial \rho}{\partial T}\right)_p$ is the coefficient of thermal expansion. The rate of strain and viscous stress tensors are given by:

$$\boldsymbol{\gamma} = \frac{1}{2}(\nabla \mathbf{v} + \nabla \mathbf{v}^t), \boldsymbol{\tau} = 2\mu\boldsymbol{\gamma} - \lambda \mathrm{tr}(\boldsymbol{\gamma})\mathbf{I}, \tag{2.3a,b}$$

where μ is the coefficient of dynamic viscosity and λ is the coefficient of second viscosity. Here, we adopt Stokes' hypothesis: μ and λ are of the same order of magnitude.

In this study, we examine the flow of two fluids, the perfect gas and the supercritical fluid obeying the van der Waals (vdW) equations of state. For a perfect gas:

$$p = \rho R T, \tag{2.4}$$

where R is the gas constant. The equation of state for a vdW fluid is:

$$p = \frac{\rho R T}{1 - b\rho} - a\rho^2, \text{where} \quad a = \frac{27}{64}\frac{R^2 T_c^2}{p_c}, b = \frac{1}{8}\frac{R T_c}{p_c}, \tag{2.5}$$

the subscript c denotes the value at the critical point. In addition [18],

$$c_p = c_{p0} + \frac{2aR(1-b\rho)\rho^2}{p - a(1-2b\rho)\rho^2}, \beta = \frac{R\rho}{p - a(1-2b\rho)\rho^2}, k = k_0\left[1 + \Lambda\left(\frac{T - T_c}{T_c}\right)^{-1/2}\right] \tag{2.6a-c}$$

where $c_{p0}$ and $k_0$ are the specific heat at constant pressure and the thermal conductivity for a perfect gas. Here, Λ is a coefficient dependent on the fluid (Λ = 0.75 for $CO_2$, for instance). The value of the exponent 0.5 is slightly less than the real critical exponent 0.57 as it is based on the mean-field theory [2,19]. However, the 0.5 exponent is convenient for our theoretical formulation and analysis for the vdW equation of state, and should not lead to a different phenomenological interpretation.

### 2.3. The general narrow-gap equations for compressible flow

We introduce dimensionless variables by using suitable scaling. We let L and H be the length scale in the streamwise and transverse directions. In this case, $\varepsilon \equiv H/L \ll 1$ is the small parameter in the analysis. We also let U and εU be the scale for the streamwise and transverse velocity components. Finally, the reference density, pressure and temperature are denoted by $\rho_r$, $p_r$ and $T_r$, respectively. Consequently, the dimensionless variables are:

$$\tilde{x} = \frac{x}{L}, \tilde{y} = \frac{y}{H}, \tilde{u} = \frac{u}{U}, \tilde{v} = \frac{v}{\varepsilon U}, \tilde{T} = \frac{T}{T_r}, \tilde{\rho} = \frac{\rho}{\rho_r}, \tilde{p} = \frac{p}{p_r}. \tag{2.7a-g}$$

$$\tilde{c}_p = \frac{c_p}{c_{pr}}, \tilde{\beta} = \frac{\beta}{\beta_r}. \tag{2.7h,i}$$

In this case, keeping leading-order terms in the stress components, equation (2.2) reduce to the following equations in the (x, y) plane (after dropping the tilde):

$$(\rho u)_x + (\rho v)_y = 0, \tag{2.8a}$$

$$\varepsilon^2 \mathrm{Re}\rho(uu_x + vu_y) = -Cp_x + u_{yy}, \tag{2.8b}$$

$$\varepsilon^4 \mathrm{Re}\rho(uv_x + vv_y) = -Cp_y, \tag{2.8c}$$

$$\varepsilon^2 \mathrm{Pec}_p \rho(uT_x + vT_y) = (kT_y)_y + \mathrm{EcPr}\, u_y^2 + \varepsilon^2 \overline{\mathrm{Pe}}\beta T u p_x, \tag{2.8d}$$

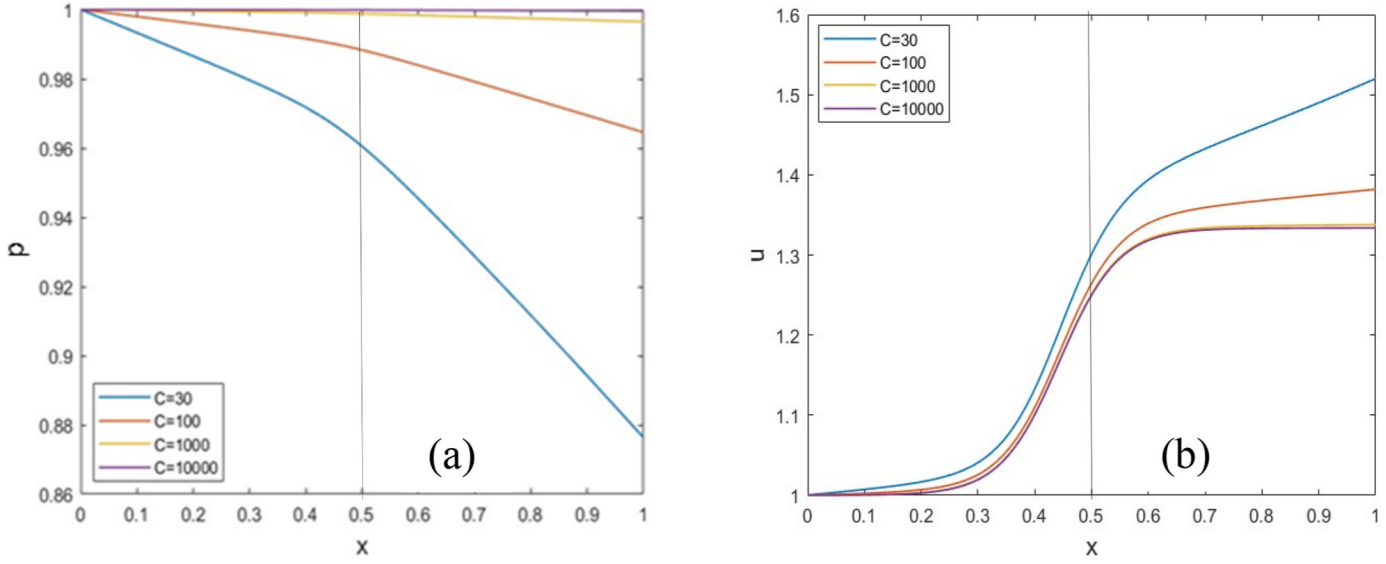


**Fig. 3.** Influence of C for an isothermal perfect gas on the (a) pressure and (b) centerline velocity profiles along the channel for the isothermal perfect gas for different values of the parameter C: C = 30, 100, 1000, 10000 and with a height reduction of 25 %. Vertical line separates the upstream and downstream regimes for C = 30.

The equations of state for perfect and vdW gases, respectively, become:

$$p = \rho T, p = \frac{\rho T}{1 - B\rho} - A\rho^2, \tag{2.9a,b}$$

where A = 9/8 and B = 1/3, and

$$c_p = 1 + E\frac{2(1 - B\rho)\rho^2}{p - A(1 - 2B\rho)\rho^2}, \beta = D\frac{\rho}{p - A(1 - 2B\rho)\rho^2}. \tag{2.9c,d}$$

where $D \equiv \frac{1}{\beta_r T_c}$ and $E \equiv A\frac{R}{c_{pr}}$. We note that expressions (2.9) for a vdW fluid are obtained by taking $p_r = \rho_c R T_c, \rho_r = \rho_c$ and $T_r = T_c$.

The various dimensionless parameters: the Reynolds number, Peclet number, Eckert number and Prandtl number, are introduced as follows:

$$Re = \frac{\rho_r UL}{\mu}, Pe = \frac{c_{pr}\rho_r UL}{k_r}, Ec = \frac{U^2}{c_{pr}T_r}, Pr = \frac{\mu c_{pr}}{k_r}, \tag{2.10a-f}$$

where $\beta_r$, $k_r$ and $c_{pr}$ are reference thermal expansion coefficient, thermal conductivity and specific heat at constant pressure, respectively. In addition, we have the ratio of the reference pressure to the reference shear stress and modified Peclet number:

$$C = \varepsilon^2\frac{p_r}{\mu U/L}, \overline{Pe} = \frac{\beta_r p_r UL}{k_r}. \tag{2.11a,b}$$

In this study, the convective forces are assumed to be negligible. In other words, we assume $Re \ll \varepsilon^{-2}$. Since $\frac{C}{\varepsilon^2 Re} = \frac{p_r}{\rho_r U^2}$, inertia effects become negligible if $p_r \gg \rho_r U^2$. It is not difficult to show that this inequality is satisfied under general flow conditions of both the perfect and vdW gases. The order of magnitude of the remaining parameters will be discussed shortly separately for the perfect and vdW gases.

### *2.4. The inertialess converging channel flow formulation*

In the absence of the convective term in (2.8b) and (2.8c), the transverse pressure gradient vanishes $\left(p_y \approx 0\right)$, and equation (2.8) reduce to:

$$(\rho u)_x + (\rho v)_y = 0, \tag{2.12a}$$

$$u_{yy} = C\frac{dp}{dx}, \tag{2.12b}$$

$$\varepsilon^2 Pec_p\rho\left(uT_x + vT_y\right) = \left(kT_y\right)_y + EcPr\, u_y{}^2 + \varepsilon^2\overline{Pe}\beta Tu\frac{dp}{dx}, \tag{2.12c}$$

In addition to the equation of state, these equations must be solved subject to the following conditions of symmetry, adherence and no-penetration at y = h(x):

$$u_y(x, y = 0) = T_y(x, y = 0) = u(x, y = h) = v(x, y = 0) = v(x, y = h) = 0. \tag{2.13a-f}$$

In this case, the velocity components are determined in terms of the pressure gradient and density, by integrating (2.12b) and (2.12a):

$$u(x, y) = \frac{C}{2}\frac{dp}{dx}\left(y^2 - h^2\right), \tag{2.14a}$$

$$v(x, y) = -\frac{1}{\rho}\frac{d}{dx}\int_0^y \rho u dy. \tag{2.14b}$$

In this study, we assume that the density is given in terms of the pressure and the average temperature over the channel width: $\langle T\rangle(x) \equiv \frac{1}{h}\int_0^h T(x, y)dy$. Thus, we write the general equation of state as $\rho = \rho(p, \langle T\rangle)$. In this case, upon substituting (2.14a) into the integral in (2.14b), we obtain a more explicit expression for v:

$$v(x, y) = -\frac{1}{\rho}\frac{C}{2}\left[\frac{d}{dx}\left(\rho\frac{dp}{dx}\right)\left(\frac{y^3}{3} - h^2 y\right) - 2\rho\frac{dp}{dx}h\frac{dh}{dx}y\right]. \tag{2.15}$$

Far upstream, we consider the flow to be fully developed Poiseuille flow with h = 1. In this case, the pressure gradient is assumed to be imposed, and is deduced from the fact that $u(x = 0, y = 0) = -\frac{C}{2}\frac{dp}{dx}(x = 0) = 1$, yielding the following conditions at x = 0:

$$\frac{dp}{dx}(x = 0) = -\frac{2}{C}, u(x = 0, y) = 1 - y^2, \rho(x = 0) = 1. \tag{2.16a-c}$$

The equation for the pressure is obtained by integrating equation (2.12a) across the film thickness, between 0 and h(x): $\int_0^h (\rho u)_x dy = -$

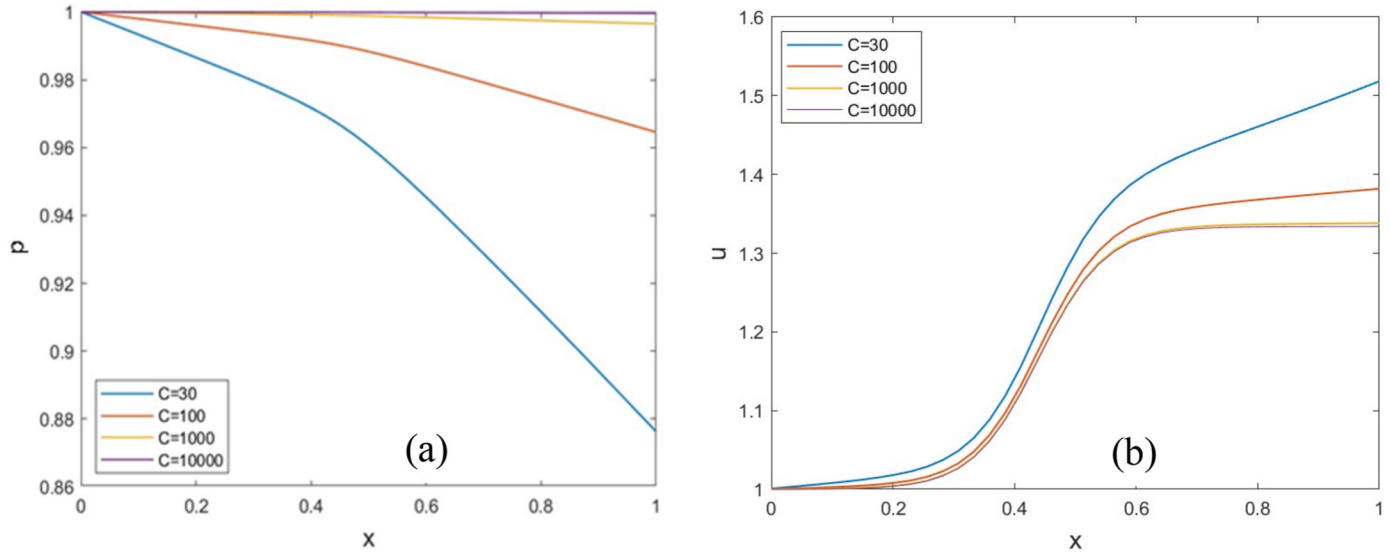


**Fig. 4.** Influence of C for a non-isothermal perfect gas on the (a) pressure and (b) centerline velocity profiles along the channel for different values of the parameter C: C = 30, 100, 1000, 10000, with EcPr = $10^{-3}$ and height reduction of 25 %.

$\int_0^h (\rho v)_y dy = \rho[v(x,y=h) - v(x,y=0)] = 0$, and using Leibniz rule to obtain $\frac{d}{dx}\left(\rho \int_0^h u dy\right) = \frac{d}{dx}\left(h^3 \rho \frac{dp}{dx}\right) = 0$. Finally, integrating this equation subject to (2.16a) yields the desired pressure gradient in terms of the density:

$$\rho \frac{dp}{dx} = -\frac{2}{Ch^3}. \tag{2.17}$$

Interestingly, when (2.17) is used, we see that both u and v are inversely proportional to the density:

$$u(x,y) = -\frac{y^2 - h^2}{\rho(x)}, v(x,y) = -\frac{3}{h^4 \rho(x)} \frac{dh}{dx}\left(\frac{y^3}{3} - h^2 y\right). \tag{2.18a,b}$$

## 3. The case of a perfect gas

### 3.1. The isothermal perfect gas

Although it is somewhat unrealistic to discuss isothermal gases, it is helpful to derive analytical results for reference. In this case T = 1 and p = ρ. The equation for the pressure (2.17) becomes:

$$p \frac{dp}{dx} = -\frac{2}{Ch^3}. \tag{3.1}$$

Interestingly, this equation suggests that the pressure gradient is negative as long as the pressure is positive, regardless of whether the channel is converging or diverging with distance. The solution is obtained subject to p (x = 0) = 1, yielding

$$p(x) = \rho(x) = \sqrt{1 - \frac{4}{C}\int_0^x h^{-3} dx}, \tag{3.2}$$

which indicates that for a contracting channel, the pressure and density decrease with distance.

Equation (3.2) is solved numerically using Matlab with 50 mesh points subject to the boundary condition p (x = 0) = 1 and a 25 % reduction in the height of the channel.

The influence of C is illustrated in Fig. 3. The C value is adjusted to 30, 100, 1000 and 10000. For C = 100, the pressure drop (Fig. 3a) across the length of the channel is about 4 %. As the value of C increases to 1000, the pressure drop is around 0.5 % and for a C value of 10000, there is almost no pressure drop as it remains almost constant all along the channel. The highest drop is for the value of C equals to 30 which corresponds to the particular case of carbon dioxide. The drop is almost 12 %, which is significant. The pressure gradient is always negative, as per equation (3.1), thus excluding any flow reversal or vortex onset.

The velocity profile is obtained from equation (2.14a) and equation (3.2). The mainstream centerline velocity u(x) is plotted for the three cases (Fig. 3b). It can be noticed that as C decreases from 10000 to 100, the velocity gradient increases at the exit. It is interesting to observe from Fig. 3 that the flow follows essentially two regimes along the channel, corresponding to the two regions close to the inlet and outlet, upstream and downstream of the vertical line shown in the two figures, illustrating the case for C = 30. Clearly, the pressure gradient remains close to constant in each regime, while the velocity changes concavity.

### 3.2. The non-isothermal perfect gas

In this case, the equation of state is: $p = \rho\langle T\rangle$, and equation (2.17) reduces to:

$$\frac{p}{\langle T\rangle}\frac{dp}{dx} = -\frac{2}{Ch^3}. \tag{3.3}$$

As to the energy equation (2.12c), both the specific heat at constant pressure as well as the coefficient of thermal expansion remain constant for any temperature and pressure so that the terms of order $\varepsilon^2$ in (2.12c) can be neglected, reducing the equation to (with k = 1):

$$T_{y_y} + EcPr\, u_y{}^2 = 0. \tag{3.4}$$

Substituting (2.14a) and integrating (3.4) subject to (2.13b) and T(x, y = h) = 1, we obtain:

$$T(x,y) = 1 - \frac{C^2 EcPr}{12}\left(\frac{dp}{dx}\right)^2 (y^4 - h^4), \langle T\rangle(x) = 1 + \frac{C^2 EcPr}{15} h^4 \left(\frac{dp}{dx}\right)^2. \tag{3.5a,b}$$

Eliminating the average temperature from (3.5b), equation (3.3) leads to a nonlinear equation for the pressure:

$$\frac{C^2 EcPr}{15} h^4 \left(\frac{dp}{dx}\right)^2 + \left(1 + \frac{4EcPr}{15}\right)\frac{C}{2} h^3 p \frac{dp}{dx} + 1 = 0. \tag{3.6}$$

As in the isothermal case, the non-isothermal perfect gas flow is

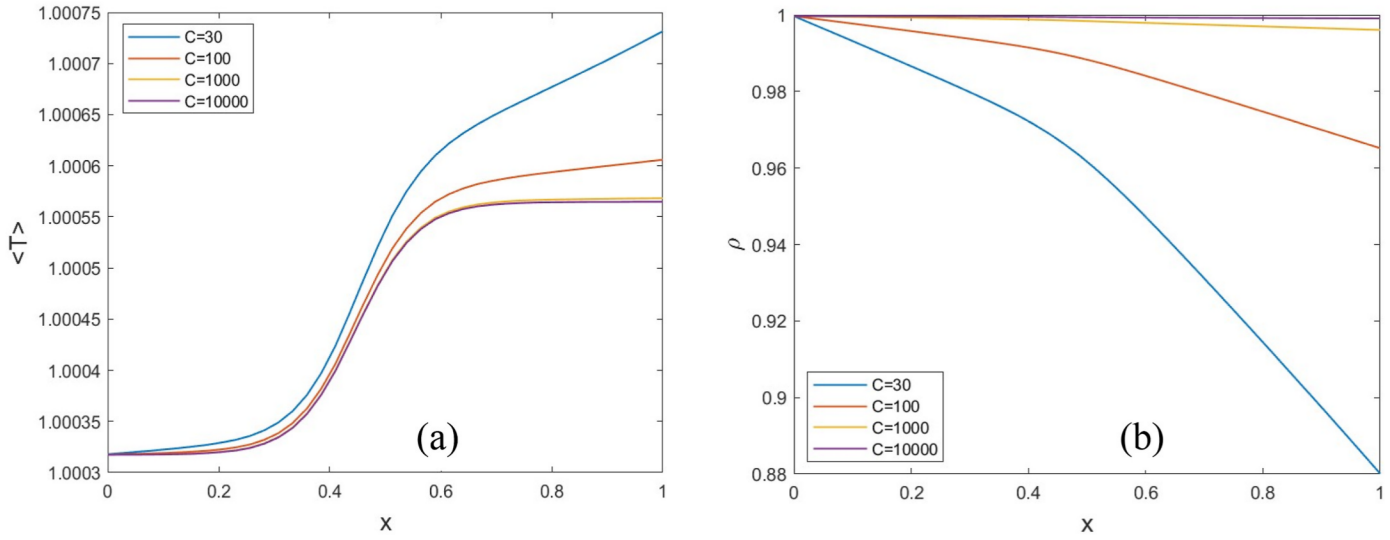


**Fig. 5.** Influence of C for a non-isothermal perfect gas on the (a) average temperature and corresponding (b) average density profiles along the channel for different values of the parameter C: C = 30, 100, 1000, 10000, with EcPr = $10^{-3}$ and height reduction of 25 %.

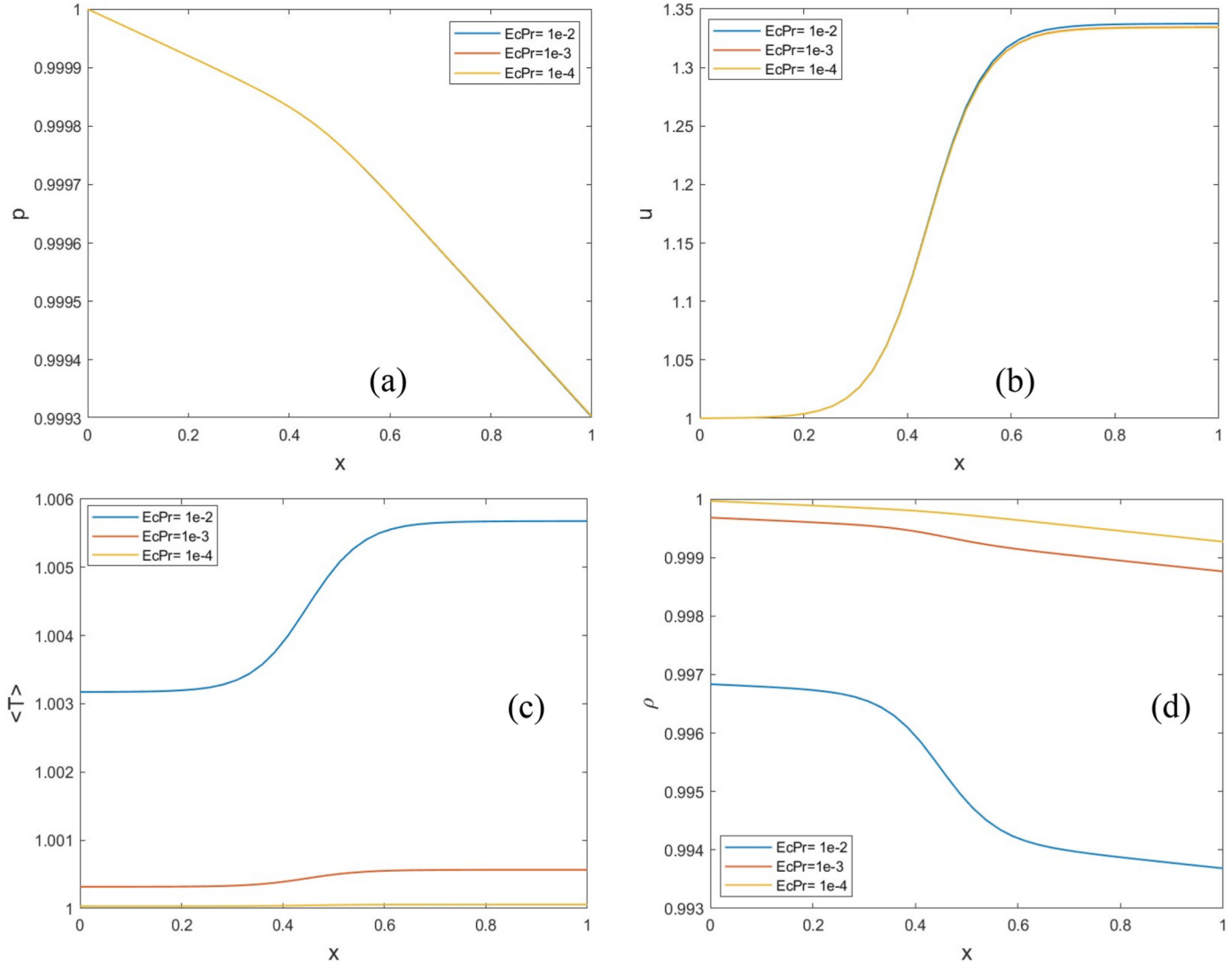


**Fig. 6.** Influence of EcPr for a non-isothermal perfect gas on (a) the pressure, (b) longitudinal velocity, (c) average temperature and (d) average density profiles along the channel for different values of the parameter EcPr, EcPr = $10^{2}$, $10^{-3}$, $10^{-4}$, and with C = 5000.

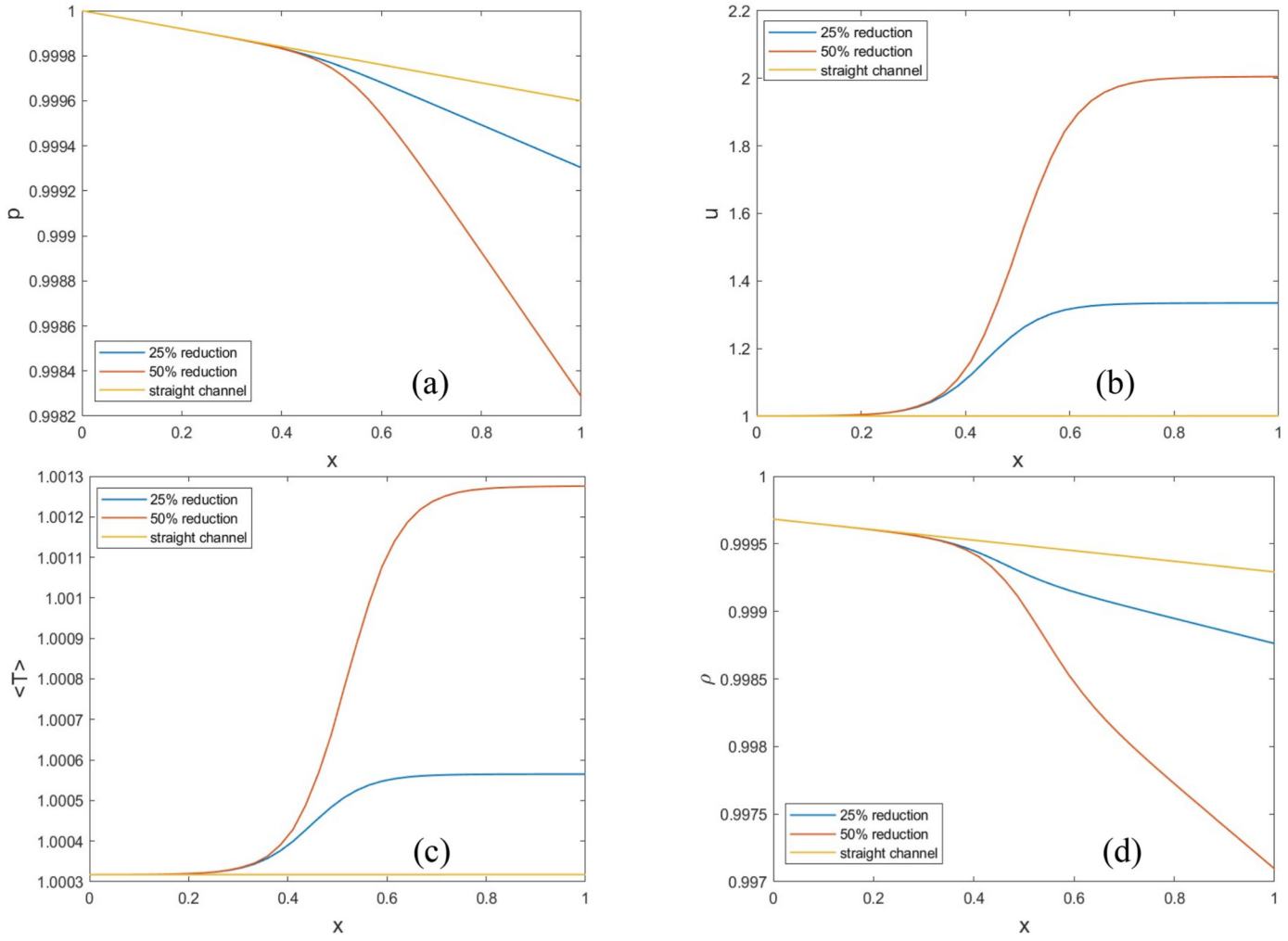


**Fig. 7.** Influence of the channel contraction for a non-isothermal perfect gas on the (a) pressure field, (b) longitudinal velocity field, (c) average temperature and (d) average density profiles along the channel for different forms of the geometry, 25 % and 50 % of reduction and a straight channel with C = 5000 and EcPr = $10^{-3}$.

obtained for the same conditions by solving equations (3.5b) and (3.6). However, unlike the isothermal case where the pressure is solved by integrating equation (3.2), the non-isothermal perfect gas pressure equation (3.6) is a second-order non-linear equation for the pressure field, which is solved using ODE45 routine in Matlab based on an explicit Runge-Kutta algorithm. As in the perfect gas case, the pressure and velocity are plotted for several values of C in Fig. 4, and the corresponding average temperature and density fields are also plotted in Fig. 5. The procedure for obtaining the solution for all fields is the following:

1) After obtaining the solution for the pressure equation (3.6), the average temperature is obtained from equation (3.5b).
2) The average density field is calculated from the $p = \rho\langle T\rangle$ (for the sake of simplicity, the $< >$ is omitted in the density field.
3) The complete temperature field can then be obtained from equation (3.5a) and the corresponding density field from the perfect gas equation: $p = \rho T$.

The non-isothermal case is dependent on an additional parameter, namely EcPr. In the following results, EcPr is taken as $10^{-3}$, its influence will be shown later.

The results show that, similar to the isothermal case, as C decreases, the pressure drop and the velocity both increase (see Fig. 4a and b). The pressure field and consequently the velocity field are essentially the same, both qualitatively and quantitatively as the isothermal gas, even though the pressure equation (3.6) is very different. The average temperature along the channel increases, which shows the role of heat dissipation (Fig. 5a), behaving similar to the velocity. As C decreases, the increase in average temperature becomes sharper; this can correspond to an increase in flow velocity for fixed properties of the fluid (see expression 2.11a, showing the inlet velocity increasing as C decreases). The density field in Fig. 5b behaves similar to the pressure field with the drop becoming higher as C decreases. For a 0.04 % increase in temperature between the inlet and outlet of the channel for C = 30, the corresponding density drop is of the order of 12 %. Finally, the upstream and downstream regimes discussed for isothermal gas are also distinct for the non-isothermal gas.

In order to assess the influence of dissipation, the C value is now kept fixed at C = 5000, $\varepsilon = 0.01$, and EcPr is varied from $10^{-2}$ to $10^{-4}$. The results in Fig. 6 show that as EcPr increases, which indicates an increase in the velocity of the mainstream for a given fluid, the pressure drop and the centerline velocity are only slightly affected. In contrast, the average temperature and density increase significantly with increasing EcPr. In particular, both the temperature and density exhibit a change in concavity with increased dissipation. It should be noted that since the average temperature and density fields are dependent on EcPr, the curves do not start from the same point at the inlet. Nevertheless, an increase of 0.5 % of the average temperature is seen with an increase of heat dissipation of hundred times (EcPr varying from $10^{-4}$ to $10^{-2}$).

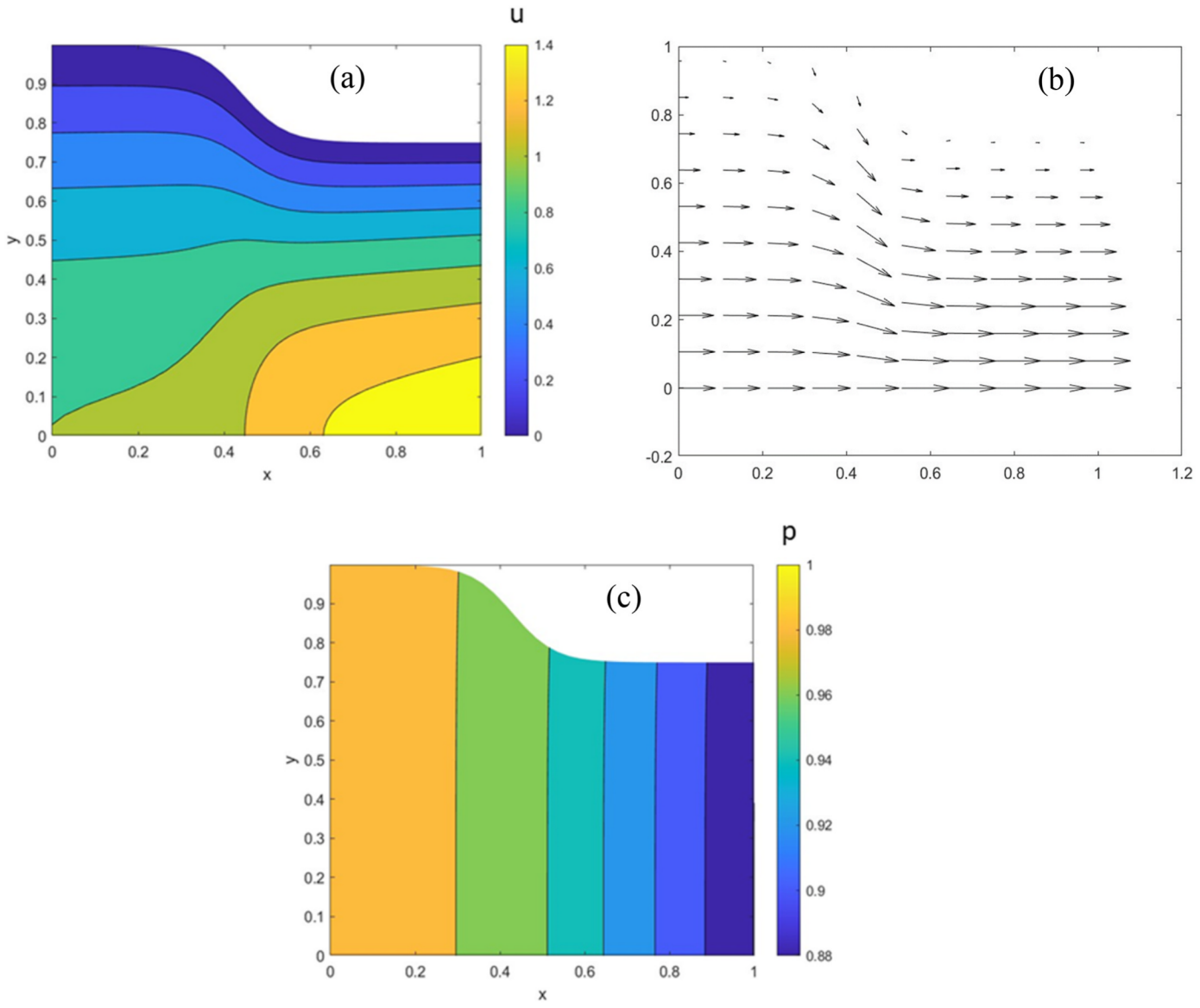


**Fig. 8.** (a) Contour plots of the longitudinal velocity field, (b) velocity vectors and (c) pressure field for the non-isothermal perfect gas for C = 30, EcPr = $10^{-3}$ and 25 % of the reduction of channel height.

The influence of the geometry is illustrated in Fig. 7. The height of the channel is modified such that if the reduction of the height is 50 %, it represents a decrease of the height from 1 to 0.5. A straight channel is also considered for a clear comparison between the constricted channel and a straight channel. As a result, the 50 % reduction in height shows the highest change in all fields. Moreover, as expected, the pressure field exhibits a linear profile for a straight channel and a non-linear evolution as the geometry changes towards the constricted form. It is interesting to observe that the effect of contraction is essentially nonexistent over a significant distance downstream of the inlet ($0< x < 0.3$), suggesting an absence of downstream influence on the flow and heat transfer.

Fig. 8 shows the contour plots of the flow field, namely the longitudinal velocity (Fig. 8a), the velocity vector field (Fig. 8b) and the pressure (Fig. 8c). The pressure contour plot shows, as expected, a horizontal variation and is constant with respect to the transverse direction. The variation of u along the centerline is stronger than any other height; this variation weakens as y increases from zero, and, as expected, becomes absent along the upper boundary. The transverse variation (along y) is most noticeable at the outlet of the channel.

The corresponding contours of the temperature and density fields are reported in Fig. 9a and b, respectively. While the temperature field is readily obtained from equation (3.5a), the density field is obtained from the perfect gas equation of state by taking $\rho(x, y) = p(x)/T(x, y)$. We recall that this is not the equation of state used in our calculations as we assumed the density $\rho = \rho(x)$ and used $p(x) = \rho(x)\langle T\rangle(x)$ as a substitute equation of state to keep the development manageable. Consequently, the contours in Fig. 9b should be considered as our attempt to recouple the density to the temperature in the (x, y) plane. Nevertheless, it is interesting to note from Fig. 9a and b that both $T(x, y)$ and $\rho(x, y)$ exhibit a weak dependence on y near the centerline, especially closer to the channel outlet. The dependence on y becomes more pronounced near the channel upper boundary with simultaneous weaker dependence on the streamwise direction.

## 4. The case of a supercritical fluid

### 4.1. *The isothermal van der Waals fluid*

In this case, we introduce the reference pressure, temperature and density as $p_r = \rho_c r T_c$, $T_r = T_c$ and $\rho_r = \rho_c$, respectively. In this

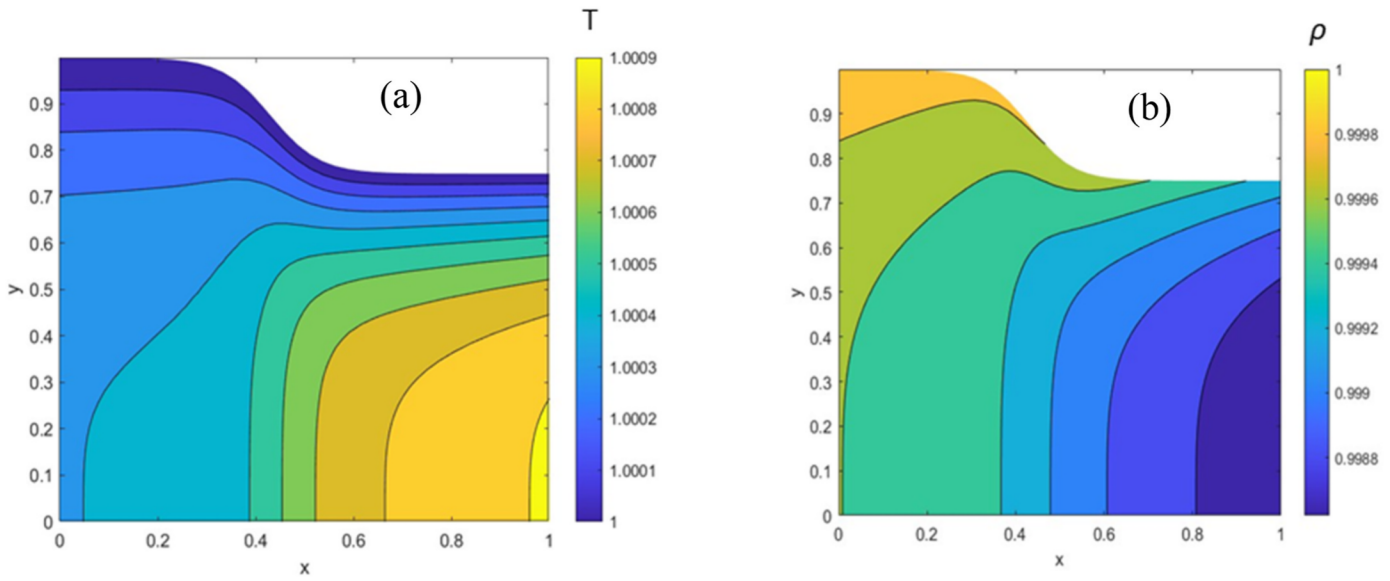


**Fig. 9.** Contour plots of (a) the temperature field and (b) density field for the non-isothermal perfect gas for C = 30, EcPr = $10^{-3}$ and 25 % of the reduction of channel height.

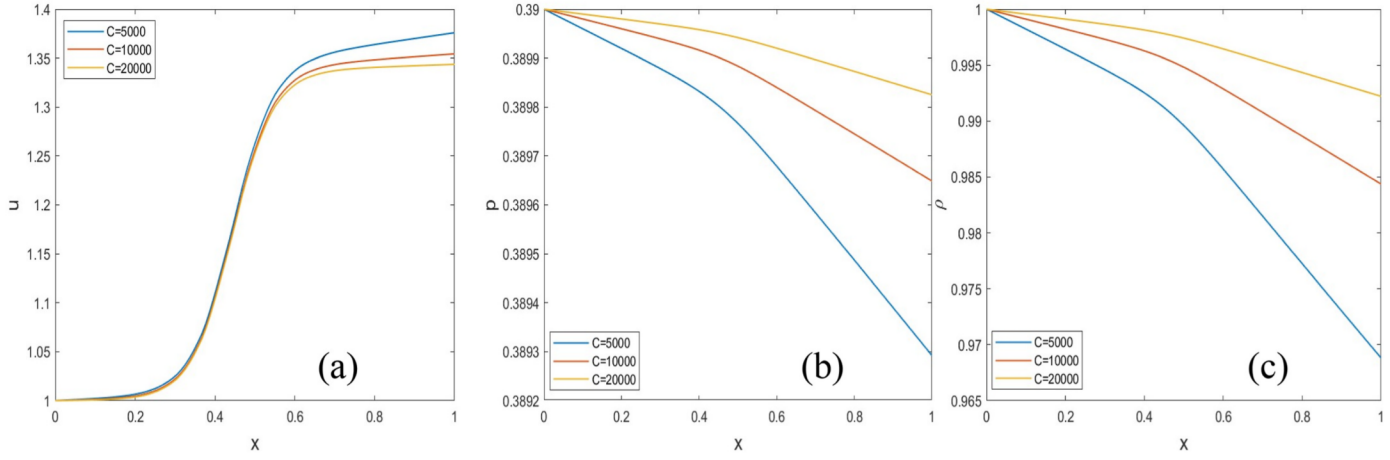


**Fig. 10.** Influence of C for isothermal vdW fluid on the (a) longitudinal velocity, (b) pressure and (c) density fields for different values of C: C = 5000, C = 10000 and C = 20000 with 25 % of the reduction of channel height.

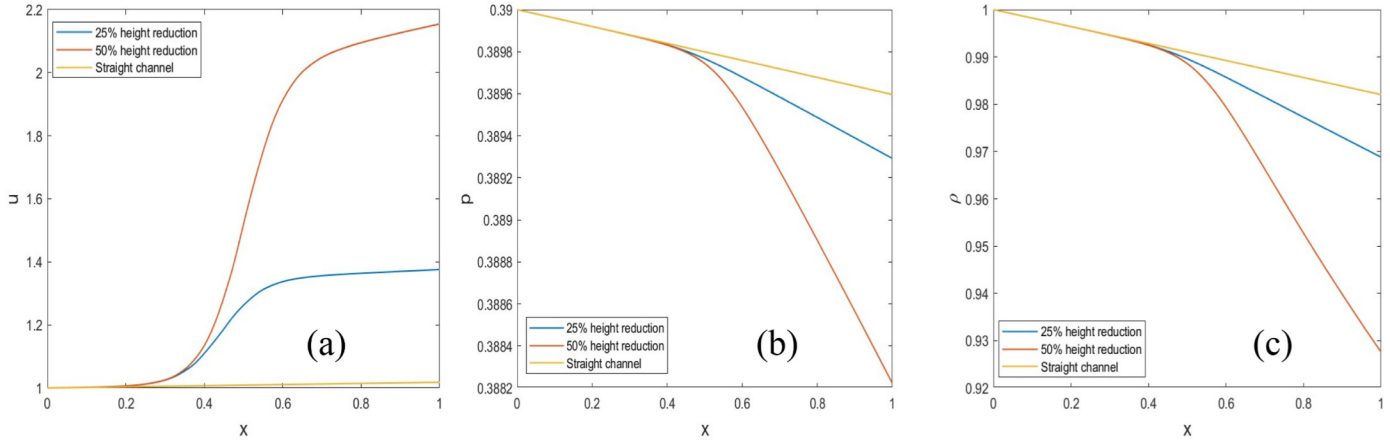


**Fig. 11.** Influence of channel contraction for isothermal vdW fluid on the (a) longitudinal velocity, (b) pressure and (c) density fields for different forms of the geometry: 25 %, 50 % of height reduction and a straight channel with C = 5000.

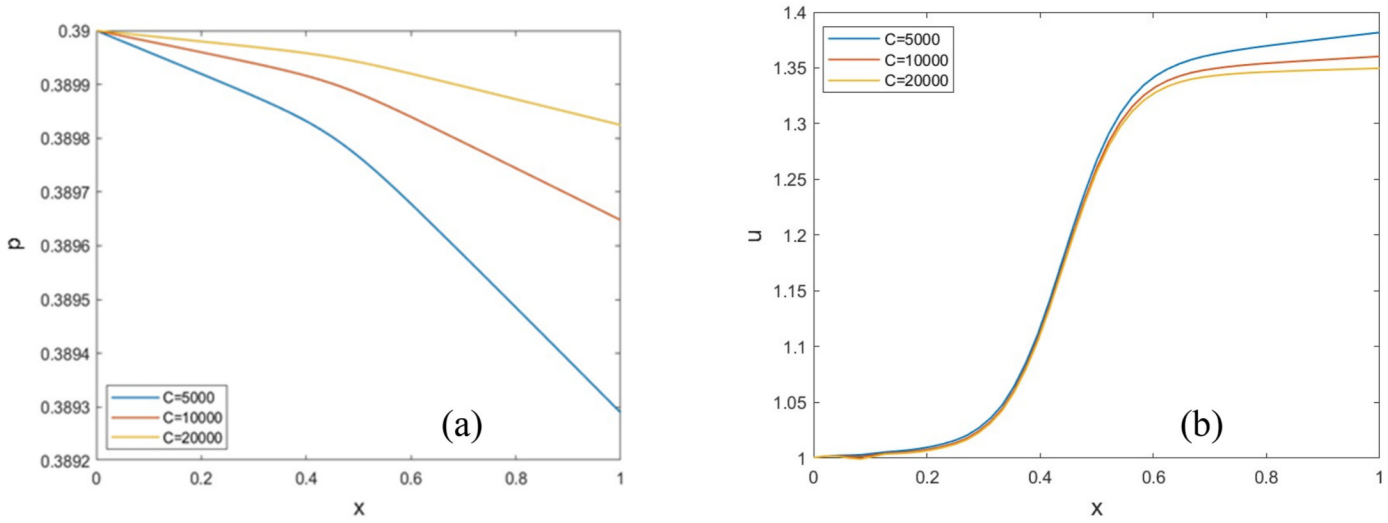


**Fig. 12.** Influence of C for the non-isothermal vdW fluid on the (a) pressure and (b) centerline velocity profiles along the channel for different values of the parameter C: C = 5000, 10000, 20000, with EcPr = $10^{-3}$, 25 % reduction in channel height and $\delta = 0.01$.

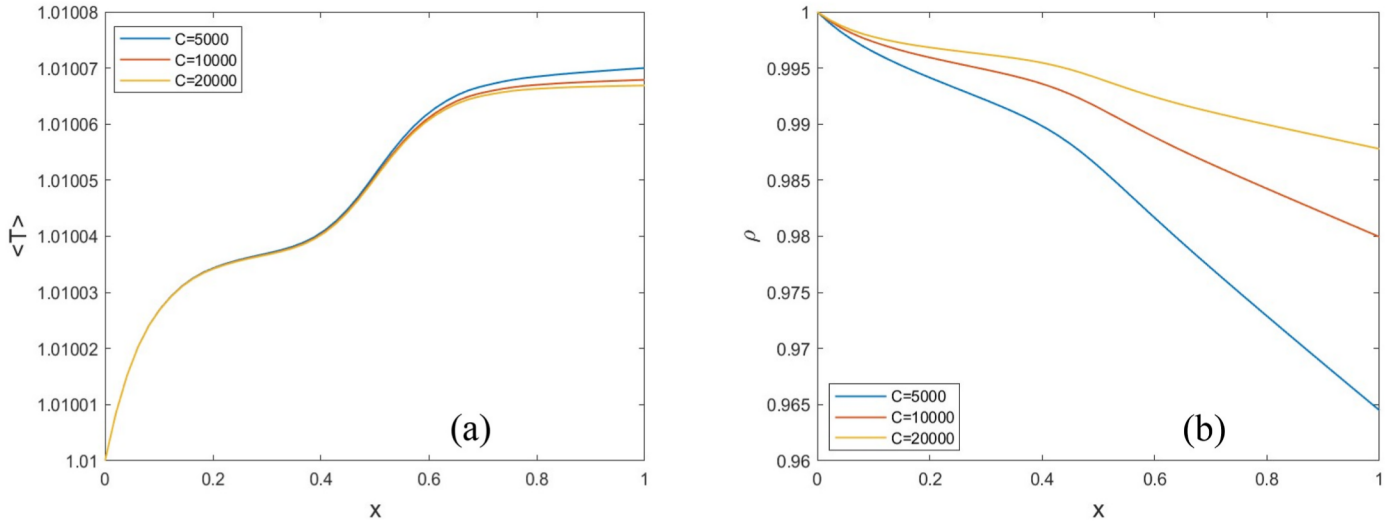


**Fig. 13.** Influence of C for the non-isothermal vdW fluid on the (a) average temperature and corresponding (b) average density profiles along the channel for different values of the parameter C: C = 5000, 10000, 20000, with EcPr = $10^{-3}$, 25 % reduction in channel height and $\delta = 0.01$. The waviness of the temperature and density is accentuated under some conditions as we shall see shortly.

(isothermal) case, we take the constant temperature to correspond to a slight deviation from the critical temperature: $T = 1 + \delta$, where $\delta \ll 1$ is a measure of the deviation from criticality. Consequently, the dimensionless form of the equation of state (2.9b) reduces to:

$$p = \frac{\rho(1+\delta)}{1-B\rho} - A\rho^2, A = \frac{9}{8}, B = \frac{1}{3}. \tag{4.1}$$

It is more convenient, given the cubic equation in ρ, to determine the density first rather than the pressure. Thus, substituting for p from (4.1) into (2.17) the equation for the density becomes:

$$\rho h^3 \left[\frac{1+\delta}{(1-B\rho)^2} - 2A\rho\right]\frac{d\rho}{dx} = -\frac{2}{C}. \tag{4.2}$$

Once the density is determined from (4.2) subject to $\rho(x=0) = 1$, the pressure is then evaluated from (4.1). In particular, $p(x=0) = \frac{1+\delta}{1-B} - A$.

Like the isothermal perfect gas case, the isothermal van der Waals case is solved for the same boundary conditions using ODE45 subroutine with an explicit Runge-Kutta algorithm in Matlab for the density field (4.2). Unlike the perfect gas, the pressure and density fields are different (p≠ρ).

The influence of C is reported in Fig. 10, where the pressure, velocity and density are plotted for C equal to 5000, 10000, and 20000. The results show that as C is decreasing, the pressure drop and the velocity increase become higher, like in perfect gas. In addition, the density behaves similar to the pressure with the drop becoming higher as C decreases. The pressure drop for a perfect gas with the value of C = 5000 gives 0.07 % which can be compared with a van der Waals with a value more than double, 0.18 %. The two regimes discussed above in relation to Fig. 4 are also visible in Fig. 10 for the velocity, pressure and density. Despite the wide range of C values, and unlike the pressure and density, the velocity is particularly insensitive to the C variation in the upstream regime; this should be contrasted with Fig. 4.

The geometry of the channel is changed such that the decrease in the height of 50 % corresponds to a reduction of the height from 1 to 0.5. The C value is kept at 5000. In addition, the straight channel case is also highlighted. The results for the three geometries (25 %, 50 % and straight channel) are plotted in Fig. 11. By comparing the results of the

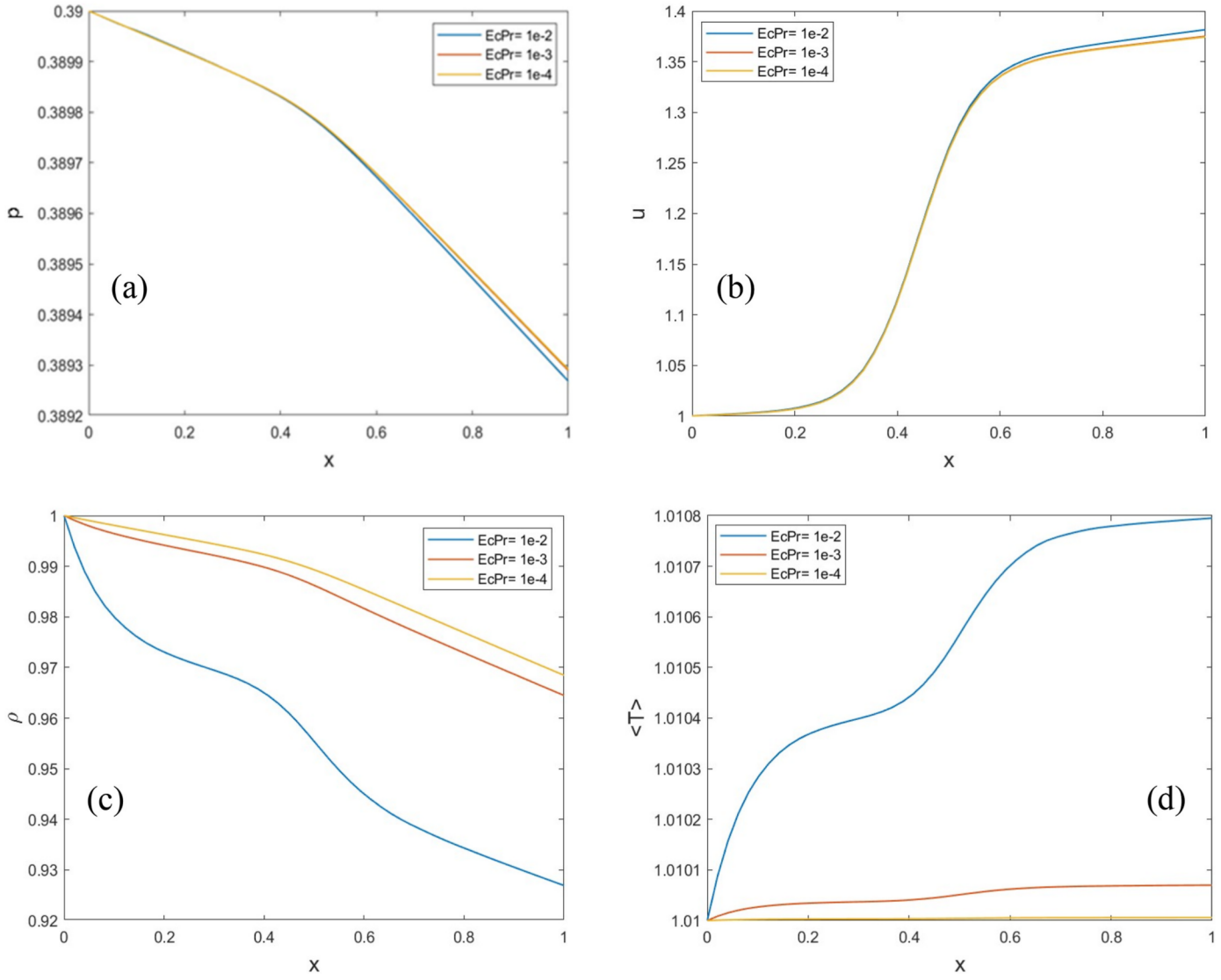


**Fig. 14.** Influence of EcPr for the non-isothermal vdW fluid on the (a) pressure, (b) centerline velocity (a) average temperature and (b) average density profiles along the channel for different values of the parameter EcPr: EcPr $= 10^{-2}$, $10^{-3}$ and $10^{-4}$, with C $= 10000$, 25 % reduction in channel height and $\delta = 0.01$.

three geometries, for the same values of C, the drop in pressure and density is the highest for the 50 % reduction in height as has also been shown in the perfect gas case. The drop in the density and pressure for the straight channel is the lowest with a linear behavior. The velocity had the highest increase for the 50 % height reduction while the velocity of the straight channel was quasi-linear. The increase in velocity magnitude is more than 200 % when compared to the increase in straight channel. In contrast to Fig. 10, both the pressure and density are insensitive to the channel contraction in the upstream regime while the velocity increases significantly with contraction close to the inlet.

### 4.2. *The non-isothermal supercritical van der Waals fluid*

In this case, we show that the problem can be reduced to a second-order system in the density and average temperature. The dimensionless form of the equation of state is now given by:

$$p = \frac{\rho\langle T\rangle}{1 - B\rho} - A\rho^2, A = \frac{9}{8}, B = \frac{1}{3}. \tag{4.3}$$

This implies that the density is to be interpreted as the density averaged over the gap. The thermal conductivity is taken to be a function of the average temperature in (2.6c), and can be written in dimensionless form as:

$$k(x) = 1 + \Lambda[\langle T\rangle(x) - 1]^{-1/2}. \tag{4.4}$$

In order to keep the development manageable, we also take the temperature in the convective terms to correspond to the average temperature. In this case, eliminating the pressure gradient using (2.17), equation (2.12c) reduces to:

$$\varepsilon^2\left(Pec_p\rho\frac{d\langle T\rangle}{dx} + \frac{\overline{P}e}{2C}\frac{\langle T\rangle\beta}{h^3\rho}\right)u = kT_{yy} + EcPr\, u_y{}^2. \tag{4.5}$$

We recall that the expressions of $c_p$ and $\beta$ are given in (2.9c-d). Substituting for u from (2.14a), and integrating (4.5) subject to the symmetry condition (2.13b) and $T(x, y = h) = 1 + \delta$, we have:

$$T(x,y) = 1 + \delta - \frac{\varepsilon^2}{8k\rho h^3}\left(Pec_p\rho\frac{d\langle T\rangle}{dx} + \frac{\overline{P}e}{2C}\frac{\langle T\rangle\beta}{h^3\rho}\right)\left(\frac{y^4}{6} - h^2y^2 + \frac{5h^4}{6}\right) - \frac{EcPr}{48k\rho^2h^6}(y^4 - h^4) \tag{4.6}$$

An equation for the average temperature is readily obtained from (4.6):

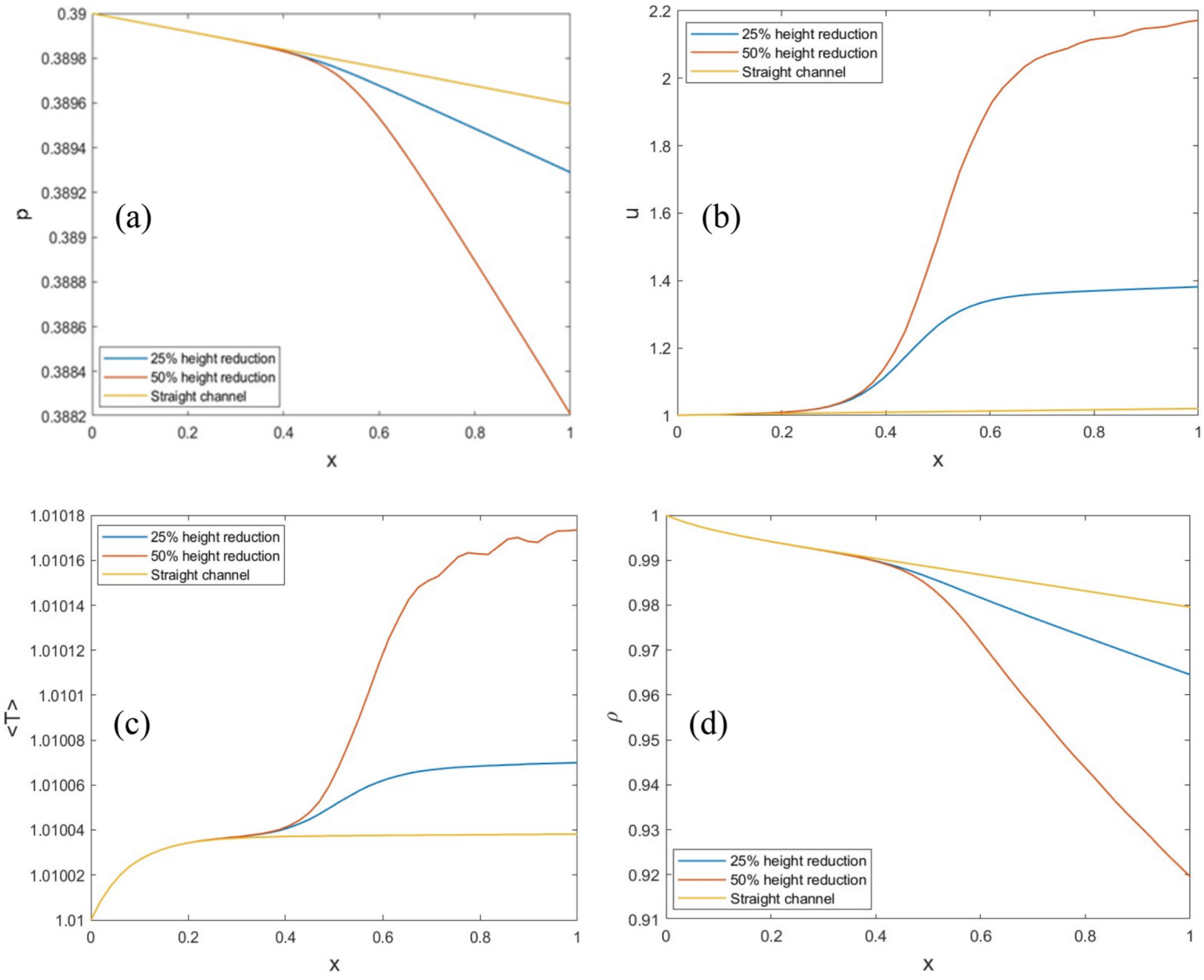


**Fig. 15.** Influence of the channel contraction on the (a) pressure, (b) centerline velocity (c) average temperature and (d) average density profiles along the channel for the non-isothermal vdW fluid for different channel geometries: 25 % height reduction, 50 % height reduction and straight channel, C = 5000, EcPr = $10^{-3}$ and δ = 0.01.

$$-\frac{\varepsilon^2 \mathrm{Pec_p h}}{15\mathrm{k}}\frac{\mathrm{d}\langle \mathrm{T}\rangle}{\mathrm{dx}} = \langle \mathrm{T}\rangle + \frac{2\varepsilon^2 \overline{\mathrm{P}}\mathrm{e}\beta\langle \mathrm{T}\rangle - \mathrm{EcPr}}{60\mathrm{kh}^2\rho^2} - 1 - \delta, \tag{4.7}$$

which indicates that $\langle \mathrm{T}\rangle > 1+\delta$ everywhere. The second equation is obtained by differentiating (4.3), and eliminating dp/dx using (2.17), yielding:

$$\left[\frac{\langle \mathrm{T}\rangle}{(1-\mathrm{B}\rho)^2} - 2\mathrm{A}\rho\right]\frac{\mathrm{d}\rho}{\mathrm{dx}} + \frac{\rho}{1-\mathrm{B}\rho}\frac{\mathrm{d}\langle \mathrm{T}\rangle}{\mathrm{dx}} = -\frac{2}{\mathrm{C}\rho \mathrm{h}^3}. \tag{4.8}$$

This system (4.7)/(4.8) is solved subject to $\rho(\mathrm{x}=0)=1$ and $\langle \mathrm{T}\rangle(\mathrm{x}=0)=1+\delta$.

The geometry is set to a 25 % decrease in the channel height. Similar to the previous cases, the control parameters C and EcPr are varied. Additionally, for the non-isothermal vdW case, the proximity to the critical point δ is another control parameter and the effect of this parameter will be shown at the end of this section. The C value is varied from 5000 to 20000 while keeping EcPr constant at $10^{-3}$, and δ at 0.01.

The influence of C is illustrated in Figs. 12 and 13, which should be compared to Figs. 4 and 5 for a perfect gas. The general trend as C increases is generally the same for both fluids. While the velocity and pressure do not present any major qualitative differences, the temperature and density exhibit additional modulation compared to the case of a perfect gas, particularly near the channel inlet. The waviness seems to extend over the entire channel length, which is especially evident from Fig. 13a for the temperature.

It should be noted that the slight variation in the pressure and temperature resulted in a significant variation in the density due to the divergence of compressibility and thermal expansion coefficients near the critical point. If we compare non-isothermal perfect gas (non-iso PG) and non-isothermal vdW (non-iso vdW), for the value of C = 10000, one can see that the density variation is vanishing for the non-iso PG case whereas the variation is non-zero for the non-iso vdW (a rough estimation gives a density variation of around 0.1 %).

The product EcPr is also varied from $10^{-2}$ to $10^{-4}$ to assess the dissipation, while keeping C constant at 10000, and δ at 0.01. The results (see Fig. 14) show that as EcPr increases, the pressure drop slightly increases while the density drop increases significantly (up to 7 % for the highest value of EcPr = $10^{-2}$). Also, the average temperature increases slightly as EcPr increases. These results are expected with the high compressibility and thermal expansion of these supercritical fluids which show high density variation with respect to small variations in

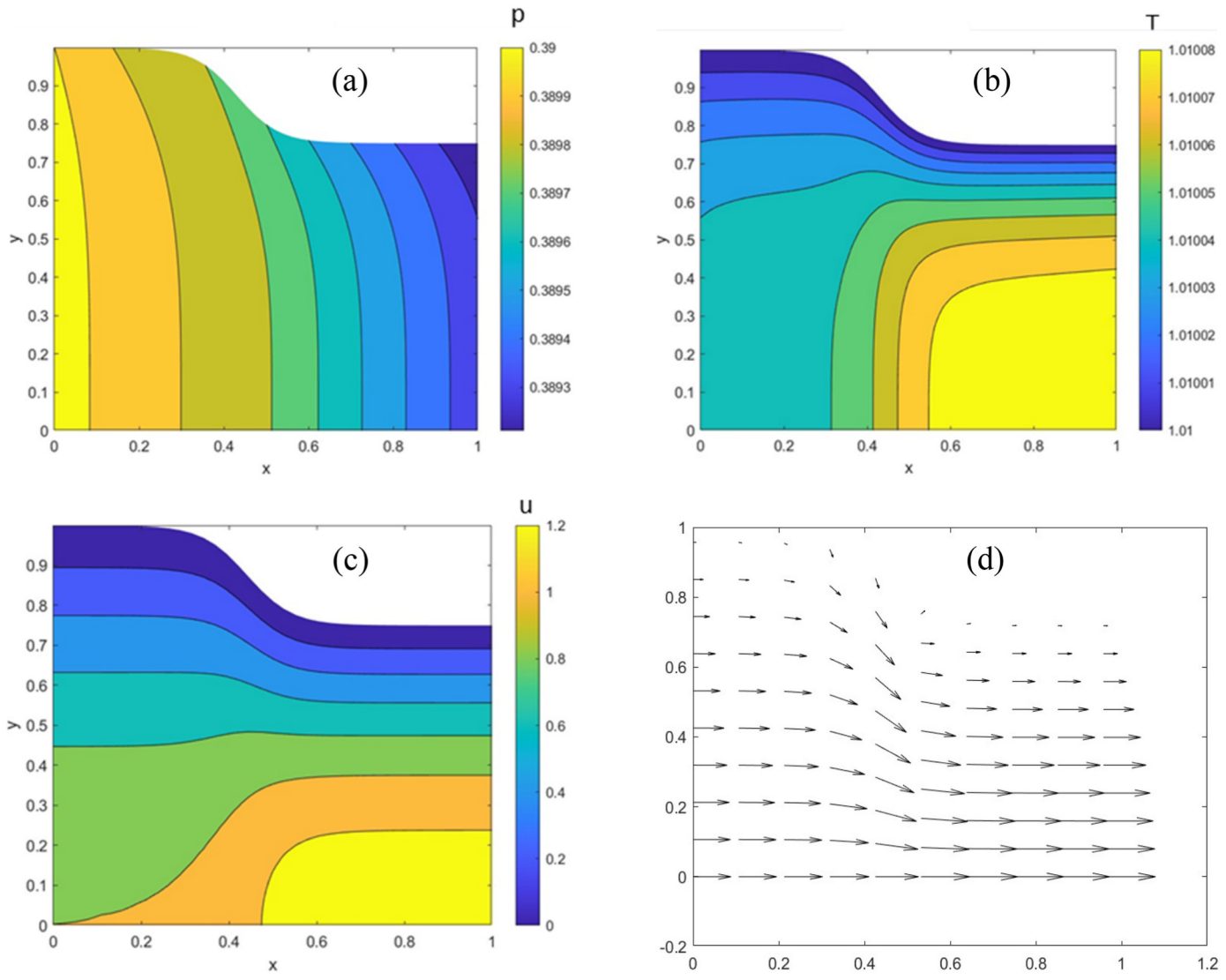


**Fig. 16.** Contour plot of (a) the pressure field (b) temperature field (c) the longitudinal velocity field and (d) velocity vector field for the non-isothermal vdW for C = 5000, EcPr = $10^{-3}$, δ = 0.01 and 25 % of the reduction of channel height.

temperature and pressure fields. While the velocity and pressure remain essentially unaffected by dissipation, the influence of EcPr on the temperature is rather significant, both qualitative and quantitative. For relatively small EcPr, both the density and temperature behaves monotonically with respect to position; the temperature tends to almost level off near the channel inlet while the density decreases. For larger EcPr, the density and temperature exhibit modulation.

The geometry of the channel is now changed such that the decrease in the height is 50 % (from 1 to 0.5). The C value is kept at 5000, EcPr = $10^{-3}$, and δ = 0.01. In addition, the channel geometry is changed to represent a straight channel. The results of the two geometries (50 % and straight channel) are plotted along with the 25 % height drop geometry (see Fig. 15). By comparing the results of the three geometries, for the same values of C, EcPr, and δ, the drop in pressure and density is the highest for the 50 % reduction in height which is in phase of the results for a perfect gas. The straight channel has the lowest pressure drop of 0.05 % while for the 25 % reduction, it is around 0.08 % and for the 50 % reduction, it is 0.2 %. Similar to the pressure, the density drop is the highest for the 50 % reduction in height (5 %) compared to the 25 % height reduction (2 %) and the straight channel (1 %). The average temperature has the highest increase for the 50 % height reduction of 0.015 % compared to the 25 % reduction of 0.007 % and the straight channel of 0.004 %.

More importantly, while the flow for the straight and mildly contracting channel exhibits smooth variation with distance, the flow exhibits oscillatory behavior or ripples for a channel with 50 % contraction. The ripples are particularly noticeable for the velocity and average temperature along the central line of the channel. It is important to note that such ripples do not arise for a perfect gas (see Fig. 11). The presence of waviness and ripples is not entirely unexpected, as they can be explained by the severe coupling between the flow and heat transfer for a vdW fluid; the coupling is particularly severe near the channel outlet in the contracted region. Mathematically, this coupling is obvious from equations (4.7) and (4.8) for the temperature and density. These equations constitute a nonlinear two-degree-of-freedom system. By eliminating the temperature or the density, it is not difficult to show that the system can be reduced to 1 s-order damped oscillatory equation with variable speed of sound and damping.

Additional insight is gained by examining the flow and thermal field distributions over the entire channel. Contour plots of the pressure, temperature and longitudinal velocity are presented in Fig. 16 in order to visualize the flow field and dissipation inside of the channel for C = 5000, EcPr = $10^{-3}$, δ = 0.01 and for a height drop of 25 %. The velocity vector field is also plotted in Fig. 15d in order to visualize the flow

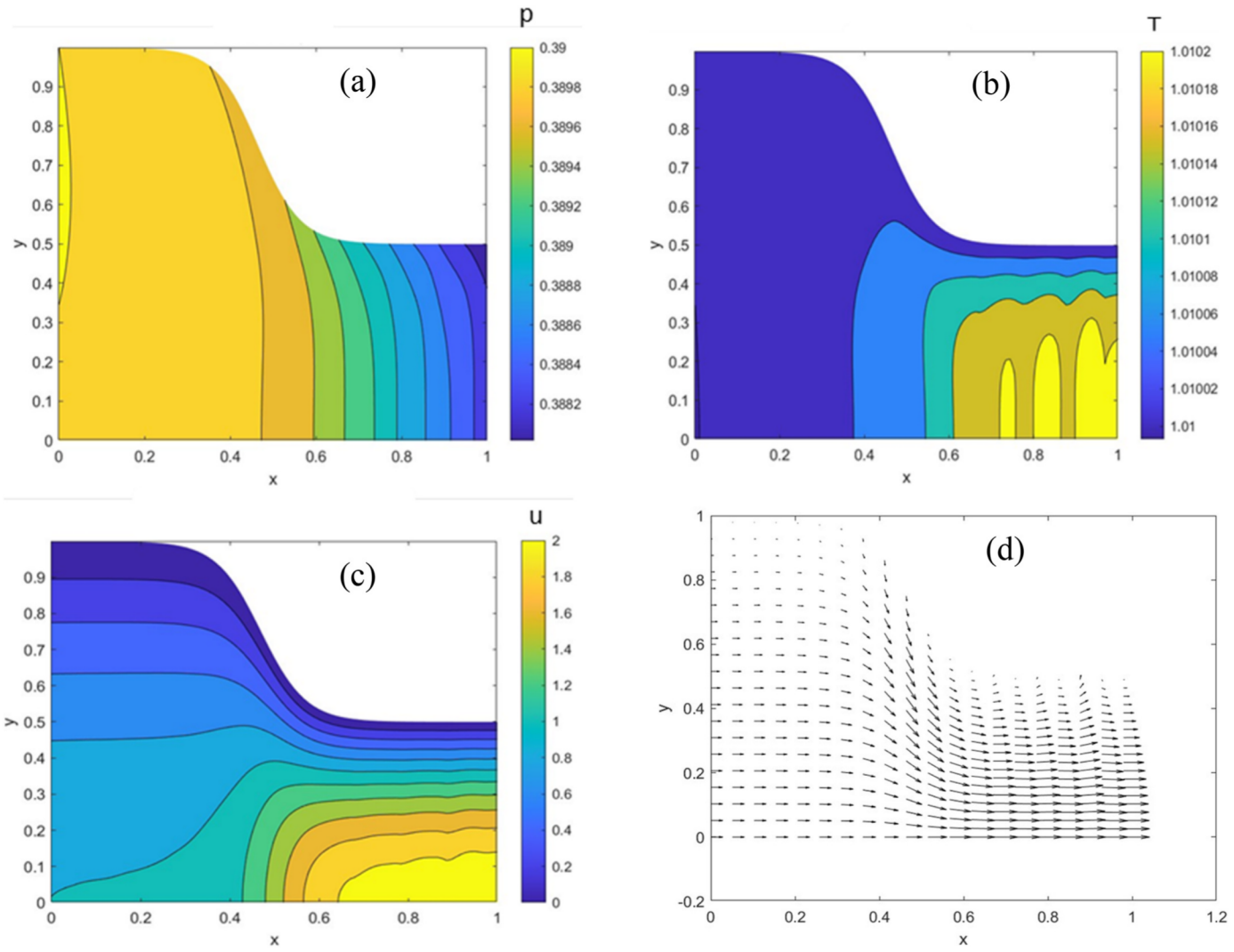


**Fig. 17.** Contour plot of (a) the pressure field (b) temperature field (c) the longitudinal velocity field and (d) velocity vector field for the non-isothermal vdW for C = 5000, EcPr = $10^{-3}$, δ = 0.01 and 50 % of the reduction of channel height.

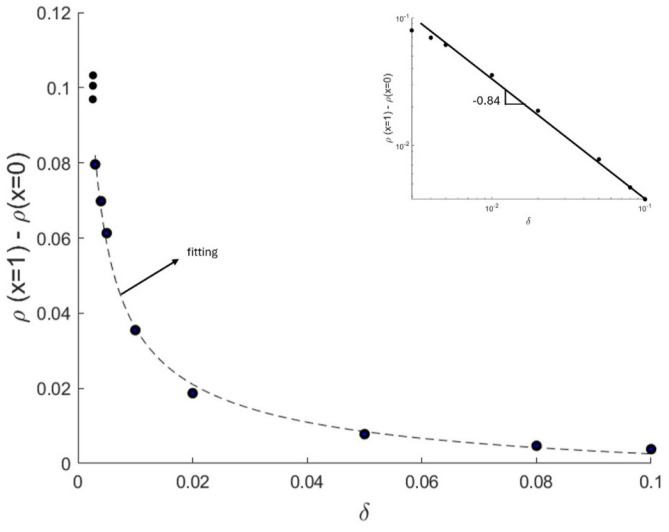


**Fig. 18.** Density drop ($\rho(x=1)-\rho(x=0)$) as a function of $\delta = \frac{T-T_c}{T_c}$ for the non-isothermal vdW fluid for C = 5000, EcPr = 0.0012 and 25 % of the reduction of channel height.

pattern inside the channel. We notice some perturbation of the flow field nearby the constriction where the slope of the channel is maximum. This physical phenomenon is further intensified for higher height drop which will be show in subsequent figures.

Contour plots of the pressure, temperature and longitudinal velocity fields (see Fig. 17) are also plotted with a higher height drop of 50 % with C = 5000, EcPr = $10^{-3}$, and δ = 0.01. While the pressure variation in Fig. 17a is smooth over the channel length, the remaining variables exhibit strong non-homogeneity in both the streamwise and transverse directions. The variation along the centerline in Fig. 17b and c is obviously related to the ripples reported earlier for the average temperature.

The proximity to the critical point δ is varied from $10^{-1}$ to $10^{-3}$ for C = 10000 and EcPr = $10^{-3}$. The effect of δ on the density drop is shown in Fig. 18. When δ = $10^{-2}$, the density drop is of the order of 2 %. When the temperature gets closer to the critical point for δ = $10^{-3}$, the density drop increases to 7.5 %. This behavior is expected since near the critical point the fluid properties change dramatically as one approaches the critical point as stated above. These divergences lead to extreme sensitivity to the density field for changes in pressure and temperature.

In order to highlight the reason of the variation of this density difference between the exit of the channel and the inlet, we refer to the article of Nichele et al. [20] where they estimated the variation of heat capacities of argon at constant volume $C_v$ and constant pressure $C_p$ near the critical point very close to the asymptotic region. They used

molecular dynamics (MD) simulation, employing the Lennard-Jones interaction potential. The fitted MD value (with some points not too close to the critical point) showed a power-law type curve of the following form: $C_p = c(\Delta T_r)^{-d} + C_{p(i.g.)}$ where c and d are non-universal parameters given in their paper for argon, $C_{p(i.g.)}$ is the heat capacity at constant pressure of an ideal gas and $\Delta T_r = \frac{T}{T_c} - 1$ is the dimensionless reduced temperature. The most important parameter here is d and its value $d = 0.8$ for their MD model, which is comparable to $d = 0.83$ based on the NIST [21] data. The slope based on relatively higher values of $\delta$ in Fig. 18 is close to the one expressed in Ref. [20] which confirms the divergence of the density difference (the corresponding fitting curve is estimated as: $\rho(x = 1) - \rho(x = 0) = A\delta^{-d} + B$, where $A = 3.17 \times 10^{-3}$ and $B = -9.5 \times 10^{-3}$); we recall that this density difference is closely linked to the compressibility of the fluid. The latter has the same critical exponent as $C_p$ or the thermal expansion coefficient $\beta$ [2,3].

## 5. Conclusion

A compressible Poiseuille flow of a supercritical fluid in a constricted narrow channel is considered in the present study. The Navier-Stokes coupled with the energy and equation of state are solved semi-analytically. The equation of state is modelled by the perfect gas and highly compressible supercritical fluid represented by the van der Waals equation. In the present study, isothermal and non-isothermal flows are considered for comparison, and results are presented in terms of longitudinal profiles of all fields. The analytical solutions are obtained for the perfect gas in the limit of lubrication theory and averaging technique in the transverse direction in order to find a solution of the coupled set of equations. For the case of a supercritical fluid (van der Waals equation), the thermal convective terms cannot be neglected because the heat capacity diverges at the critical point; $\varepsilon^2 C_p$ can be of the order of one or even larger depending on the proximity to the critical point. Additional difficulties appeared with other properties as one approaches the critical point since the heat conductivity and thermal expansion both diverge. The resolution of these complex equations could be achieved by averaging the equations in the transverse direction.

In the results, besides the expected non-linear profiles observed in a constricted channel compared to a straight channel, two main conclusions can be drawn when looking at the results:

- The density difference between the exit and the inlet of the channels increases drastically with the distance to the critical point, and is in accordance with the literature.
- We noticed some perturbation in terms of waviness of the flow field and thermal fields near the constriction where the slope of the channel is maximum. This phenomenon is explained by the severe coupling between the flow and heat transfer for a van der Waals fluid; the coupling is particularly severe near the channel outlet in the contracted region. Mathematically, this coupling is obvious from the temperature and density equations which constitute a nonlinear two-degree-of-freedom system.

The present study opens up studies in many applications such as turbomachinery, the management of supercritical fluids in space industry, heat-exchangers in refrigeration systems to cite a few. To our knowledge, this study of an analytical solution of coupled non-linear transport equations is unique and may interest scientists and industrial partners for a quick solution in their applications without any numerical simulation or experimental tests.

## CRediT authorship contribution statement

**Abdallah El Malki:** Visualization, Validation, Software. **Roger E. Khayat:** Writing – review & editing, Writing – original draft, Methodology, Investigation, Conceptualization. **Sakir Amiroudine:** Writing – review & editing, Writing – original draft, Validation, Supervision, Methodology, Investigation, Funding acquisition.

## Declaration of competing interest

The authors declare that they have no known competing financial interests or personal relationships that could have appeared to influence the work reported in this paper.

## Acknowledgments

For the financial support, SA feels grateful to the Centre National d'Etudes Spatiales, France through the GDR MFA; REK would like to acknowledge the financial support of ENSAM and NSERC.

## Data availability

Data will be made available on request.

## References

[1] H.E. Stanley, Introduction to Phase Transitions and Critical Point Phenomena, Oxford University Press, Oxford, 1971.
[2] P. Carlès, A brief review of the thermophysical properties of supercritical fluids, J. Supercrit. Fluids 53 (1–3) (2010) 2–11.
[3] B. Zappoli, D. Beysens, Y. Garrabos, Heat Transfers and Related Effects in Supercritical Fluids, Springer, 2016.
[4] K. Nitsche, J. Straub, The critical"HUMP" of Cv under Microgravity: Results from D1-Spacelab Experiment "Wärmekapazität, 1987. ESA SP 256.
[5] H. Boukari, J.N. Shaumeyer, M.E. Briggs, R.W. Gammon, Critical speeding up in pure fluids, Phys. Rev. A 41 (1990) 2260.
[6] B. Zappoli, D. Bailly, Y. Garrabos, B. Le Neindre, P. Guenoun, D. Beysens, Anomalous heat transport by the piston effect in supercritical fluids under zero gravity, Phys. Rev. A 41 (1990) 2264.
[7] A. Onuki, R.A. Ferrell, Adiabatic heating effect near the gas-liquid critical point, Phys. A Stat. Mech. Appl. 164 (1990) 245.
[8] E. Boyko, H.A. Stone, Pressure-driven flow of the viscoelastic Oldroyd-B fluid in narrow non-uniform geometries: analytical results and comparison with simulations, J. Fluid Mech. 936 (2022) A23.
[9] J.P. Rothstein, G.H. McKinley, Extensional flow of a polystyrene Boger fluid through a 4: 1: 4 axisymmetric contraction/expansion, J. Non-Newtonian Fluid Mech. 86 (1–2) (1999) 61–88.
[10] G. Zeng, L. Chen, H. Yuan, Numerical model development for critical region flow and thermodynamic transitions of CO2 fluids in microchannel, Int. Commun. Heat Mass Tran. 150 (2024) 107204.
[11] L. Chen, G. Zeng, D. Yang, H. Yuan, J. Zang, Y. Huang, Quantitative visualization on boundary heat transfer of supercritical $CO_2$ mini-channel through-flow (Re=104) via pixelated phase-shifting interferometry, Int. J. Heat Mass Tran. 223 (2024) 125258.
[12] Martin T. White, Giuseppe Bianchi, Lei Chai, Savvas A. Tassou, Abdulnaser I. Sayma, Review of supercritical CO2 technologies and systems for power generation, Appl. Therm. Eng. 185 (2021) 116447.
[13] H. Ockendon, J.R. Ockendon, Viscous Flow, Cambridge University Press, 1995.
[14] G.G. Giusteri, R. Seto, A theoretical framework for steady-state rheometry in generic flow conditions, Journal of rheology (New York : 1978) 62 (3) (2018) 713–723. -05.
[15] J. Hinch, E. Boyko, H. Stone, Fast flow of an Oldroyd-B model fluid through a narrow slowly varying contraction, Journal of fluid mechanics 988 (2024). -05 Article A11.
[16] S. Kadia, I.A. Sofia Larsson, M. Billstein, L. Lia, E. Pummer, Supercritical flow characteristics in a narrow channel bend, in: Proceedings of the 40th IAHR World Congress, 2023. Vienna.
[17] F. Durst, Fluid Mechanics: an Introduction to the Theory of Fluid Flows, Springer, Berlin, 2008.
[18] R. Khelalfa, P.-O. Logerais, J.-F. Durastanti, J.-S. Darrozès, Study of fluid flow passing through the vicinity of the critical point, J. Thermophys. Heat Tran. 28 (2) (2014) 303–312.
[19] Y. Kulkarni, R. Khayat, S. Amiroudine, On the long-time transient formation of sink zones in near-critical fluids. A theoretical perspective, J. Fluid Mech. 915 (2021) A117.
[20] J. Nichele, A.B. de Oliveira, L.S. de B. Alves, I. Borges, Accurate calculation of near-critical heat capacities CP and CV of argon using molecular dynamics, J. Mol. Liq. 237 (2017) 65–70.
[21] NIST, Thermophysical Properties of Pure Fluids Database. NIST12, NIST, Gaithersburg MD, 2000.